Proceedings of the 2005 IEEE
International Conference on Robotics and Automation
Barcelona, Spain, April 2005

On the Biomimetic Design of the Berkeley Lower Extremity Exoskeleton (BLEEX)

Andrew Chu, H. Kazerooni, and Adam Zoss
Human Engineering & Robotics Laboratory
University of California, Berkeley, CA 94720, USA
exo@berkeley.edu

***Abstract*— Many places in the world are too rugged or enclosed for vehicles to access. Even today, material transport to such areas is limited to manual labor and beasts of burden. Modern advancements in wearable robotics may make those methods obsolete. Lower extremity exoskeletons seek to supplement the intelligence and sensory systems of a human with the significant strength and endurance of a pair of wearable robotic legs that support a payload. This paper outlines the use of Clinical Gait Analysis data as the framework for the design of such a system at UC Berkeley.**

***Index Terms*—BLEEX, Legged Locomotion, Lower Extremity Exoskeleton, Biomemetic, Clinical Gait Analysis**

I. Introduction

Material transport has been dominated by wheeled vehicles, but many environments such as stairs are simply too treacherous for them to negotiate. Many attempts have been made to develop legged robots capable of navigating such terrain [1]. Unfortunately, difficult terrain taxes not only the kinematical capabilities of such systems, but also the sensory, path planning, and balancing abilities of even the most state-of-the-art robots. Lower extremity exoskeletons seek to circumvent the limitations on autonomous legged robots by adding a human operator to the system. These systems augment human strength and endurance during locomotion. The first load-carrying, field-operational and energetically autonomous lower extremity exoskeleton was designed and built at Berkeley and is commonly referred to as BLEEX. It consists of two powered anthropomorphic legs, a power unit, and a backpack-like frame on which heavy loads can be mounted. This system allows its wearer to carry significant loads with minimal effort. Because the pilot can do this for extended periods of time without reducing his/her agility, the BLEEX increases the physical effectiveness of the pilot. In this initial model, BLEEX offers a payload capacity of seventy five pounds, with any excess payload being supported by the pilot. The BLEEX lets soldiers, disaster relief workers, firefighters, and other emergency personnel carry major loads without the strain associated with demanding labor. It is our vision that the BLEEX will provide a versatile *load transport platform* for mission-critical equipment.

II. Prior Research Work

Although autonomous robotic systems perform remarkably in structured environments like factories, integrated human-robotic systems are superior in unstructured environments that demand significant adaptation. In our research work at Berkeley, the problems of upper- and lower-extremity human power augmentation were tackled separately. The reasons for this were two-fold; firstly, there are many immediate applications for stand-alone lower- and upper-extremity exoskeletons. Secondly, exoskeleton research is still in its early stages, and further research is required before integration of upper- and lower-extremity exoskeletons can be attempted.

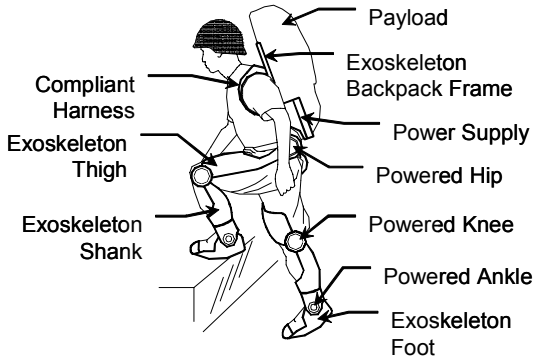

Fig. 1. Initial lower extremity exoskeleton concept at Berkeley. The architecture mimics its human wearer with connections at the wearer's feet and back only. By appropriately actuating joints, the lower extremity exoskeleton supports the payload and removes the weight from the wearer while allowing the wearer to control the balance and motion of the device.

In the mid-1980s, we initiated several research projects on upper extremity exoskeleton systems, billed as "human extenders." The main function of these was human power augmentation for manipulation of heavy and bulky objects ([12], [13], [14], and [15]). When a worker uses an upper extremity exoskeleton to move a load, the device bears the bulk of the weight while transferring a scaled-down load to the user. In this fashion, the worker can still sense the load's weight and judge his/her movements accordingly, but the force he/she feels is greatly reduced. Since upper extremity exoskeletons are mostly used for factory floors, warehouse, and distribution centers, they are hung from overhead cranes. Lower extremity exoskeletons focus on supporting and carrying heavy payloads on the operator's back (like a backpack) during long distance locomotion.

In the early 1960s, the Defense Department expressed interest in the development of a man-amplifier, a "powered suit of armor" which would augment soldiers' lifting and carrying capabilities. In 1962, the Air Force had the Cornell Aeronautical Laboratory study the feasibility of using a master-slave robotic system as a man-amplifier. In later work, Cornell determined that an exoskeleton, an external structure in the shape of the human body which has far

fewer degrees of freedom than a human, could accomplish most desired tasks [26]. From 1960 to 1971, General Electric developed and tested a prototype man-amplifier, a master-slave system called the Hardiman ([22], [23], [24], [25], and [27]). The Hardiman was a set of overlapping exoskeletons worn by a human operator. The outer exoskeleton (the slave) followed the motions of the inner exoskeleton (the master), which followed the motions of the human operator. All these studies found that duplicating all human motions and using master-slave systems were not practical. Additionally, difficulties in human sensing and system complexity kept it from walking.

Several exoskeletons were developed at the University of Belgrade in the 60's and 70's to aid paraplegics [2] and [3]. Although these early devices were limited to predefined motions and had limited success, balancing algorithms developed for them are still used in many bipedal robots [4]. The "RoboKnee" is a powered knee brace that functions in parallel to the wearer's knee and transfers load to the wearer's ankle (not to the ground) [28]. "HAL" is an orthosis, connected to thighs and shanks, that moves a patient's legs as a function of the EMG signals measured from the wearer ([29] and [30]).

The Berkeley Lower Extremity Exoskeleton (BLEEX) is not an orthosis or a brace; unlike the above systems it is designed to carry a heavy load by transferring the load weight to the ground (not to the wearer). BLEEX has four new features. First, a novel control architecture was developed that controls the exoskeleton through measurements of the exoskeleton itself [18]. This eliminated problematic human induced instability [15] and [19] due to sensing the human force. Second, a series of high specific power and specific energy power supplies were developed that were small enough to make BLEEX a true field-operational system [17]. Third, a body LAN (Local Area Network) with a special communication protocol and hardware were developed to simplify and reduce the cabling task of all the sensors and actuators needed for exoskeleton control [20] and [21]. Finally, a flexible and versatile architecture was chosen to decrease complexity and power consumption. This paper gives an overview of the biomimetic design of this architecture.

III. Exoskeleton Architecture

An anthropomorphic architecture with similar kinematics to a human was chosen for BLEEX. Thus, the exoskeleton has ankle, knee, and hip joints similar to human legs. BLEEX rigidly attaches to the operator at the feet via custom boots and bindings and at the torso through a custom vest. Other connections between pilot and device were allowed, but only if they were compliant so load does not transfer to the pilot. The exoskeleton legs can therefore follow the human's, but are not required to match exactly since there are only two rigid attachments between human and exoskeleton. The connection at the torso is made using a custom vest which allows the distribution of the forces between BLEEX and the pilot, thereby preventing abrasion. These vests are made of several hard surfaces that are compliantly connected to each other using thick fabric. The vests include rigid plates on their backs for connection to BLEEX spine. Each BLEEX leg has three degrees of freedom at the hip, one degree of freedom at the knee, and three degrees of freedom at the ankle. Both the flexion-extension and abduction-adduction degrees of freedom at the hip are actuated, as is one flexion-extension degree of freedom at the knee, and the ankle plantar-dorsi flexion (in the sagittal plane). The other three degrees of freedom (i.e., rotation and abduction-adduction at the ankle and rotation at the hip) are equipped with passive impedances using steel springs and elastomers. In total, each BLEEX leg has four powered degrees of freedom: hip joint, knee joint and ankle joint in sagittal plane and a hip abduction-adduction joint. In comparison with the movements in the sagittal plane, the actuators for hip abduction-adduction movements input less energy into the system. This article concerns with the BLEEX biomimetic design in the sagittal plane.

IV. Design by Biological Analogy

A. Clinical Gait Analysis (CGA) Data

Since we intended to design an anthropomorphic exoskeleton with similar limb masses and inertias to a human, the required joint torques and power for the exoskeleton to perform a given motion were approximated as that required by a similarly sized human performing the same motion. Additionally, since the primary goal of a lower-extremity exoskeleton is locomotion, the joint torque and power requirements for the BLEEX were thus determined by analyzing the walking cycle shown in Fig. 2.

Human joint angles and torques for a typical walking cycle were obtained in the form of independently collected Clinical Gait Analysis (CGA) data. CGA angle data is typically collected via human video motion capture. CGA torque data is calculated by estimating limb masses and inertias and applying dynamic equations to the motion data. Given the variations in individual gait and measuring methods, three independent sources of CGA data ([8], [9] and [10]) were utilized for the analysis and design of BLEEX. This data was modified to yield estimates of exoskeleton actuation requirements. The modifications included: 1) scaling the joint torques to a 75 kg person (the projected weight of BLEEX and its payload not including its pilot); 2) scaling the data to represent the walking speed of one cycle per second (or about 1.3 m/s); and 3) adding the pelvic tilt angle (or lower back angle depending on data available) to the hip angle to yield a single hip angle between the torso and the thigh as shown in Fig. 3. This accounts for the reduced degrees of freedom of the exoskeleton. The following sections describe the use of CGA data and its implication for the exoskeleton design. The sign conventions used are shown in Fig. 3.

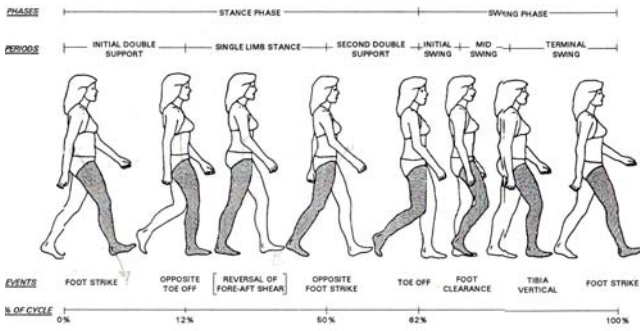

Fig. 2. The cycle begins with the start of stance phase (heel-strike) followed by toe-off and swing phase beginning at ~60% of the cycle [5].

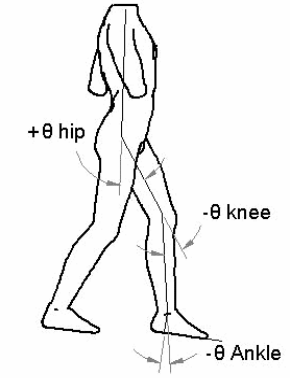

Fig. 3: Each joint angle is measured as the positive counterclockwise displacement of the distal link from the proximal link (zero in standing position) with the person oriented as shown. In the position shown, the hip angle is positive whereas both the knee and ankle angles are negative. Torque is measured as positive acting counterclockwise on the distal link.

B. The Ankle

Fig. 4 shows the CGA ankle angle data for a 75 kg human walking on flat ground at approximately 1.3 m/s vs. time. Although Fig. 4 shows a small range of motion while walking (approximately -20° to +15°), greater ranges of motion are required for other movements. An average person can flex their ankles anywhere from -38° to +35° [6]. The BLEEX ankle was chosen to have a maximum flexibility of ±45° to compensate for the lack of several smaller degrees of freedom in the exoskeleton foot. Through all plots, TO stands for "Toe-Off" and HS stands for "Heel-Strike".

Fig. 5 shows the adjusted CGA data of the ankle flexion/extension torque. The ankle torque is almost entirely negative – making unidirectional actuators an ideal actuation choice. This asymmetry also implies a preferred mounting orientation for asymmetric actuators (one sided hydraulic cylinders). Conversely, if symmetric bi-directional actuators are considered, spring-loading would allow the use of low torque producing actuators. Although the ankle torque is large during stance, it is negligible during swing. This suggests a system that disengages the ankle actuators from the exoskeleton during swing to save power.

The instantaneous ankle mechanical power (shown in Fig. 6) is calculated by multiplying the joint angular velocity (derived from Fig. 4) and the instantaneous joint torque (Fig. 5). The ankle absorbs energy during the first half of the stance phase and releases energy just before toe off. The average ankle power is positive, indicating that power production is required at the ankle.

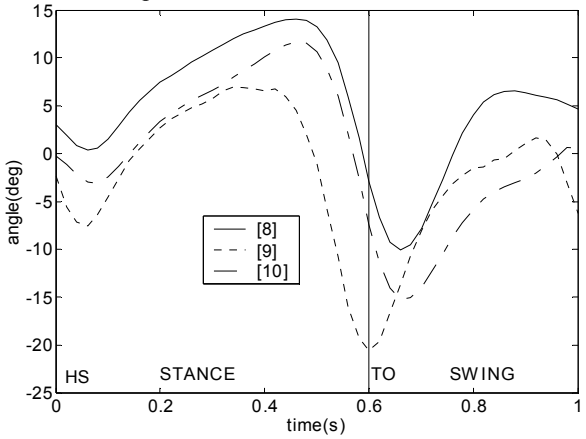

Fig. 4. Adjusted CGA data of the ankle flexion/extension angle. The minimum angle (extension) is ~-20˚ and occurs just after toe-off. The maximum angle (flexion) is ~+15˚ and occurs in late stance phase.

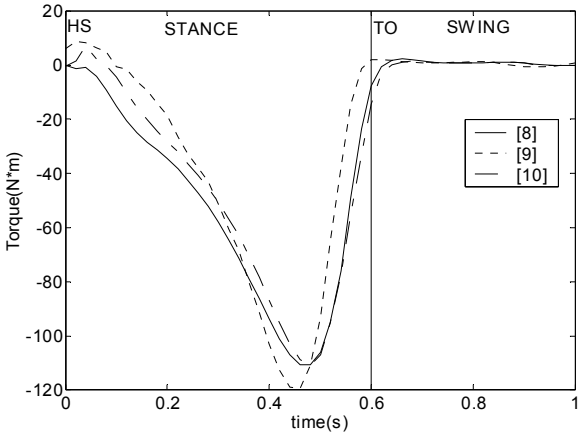

Fig. 5. Adjusted CGA data of the ankle flexion/extension torque. Peak negative torque (extension of the foot) is very large (~-120 N·m) and occurs in late stance phase. The ankle torque during swing is quite small.

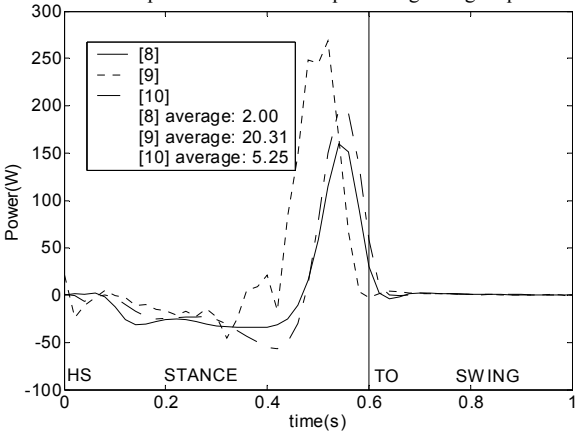

Fig. 6. Adjusted CGA data of the ankle flexion/extension instantaneous mechanical power. The average ankle power is positive, indicating the ankle does positive work and requires actuation.

C. The Knee

The knee angle in Fig. 7 is characterized by knee flexion to create a horizontal hip trajectory. The knee buckles momentarily in early stance to absorb the impact of heel strike then undergoes a large flexion during swing. This

knee flexion decreases the effective leg length, allowing the foot to clear the ground when swinging forward. Although the walking knee flexion is limited to approximately 70˚, the human has significantly more flexibility (up to 159˚ flexion possible when kneeling) [6]. The BLEEX knee flexion range was chosen to be 5° to 126°. The CGA based knee actuation torque is shown in Fig. 8.

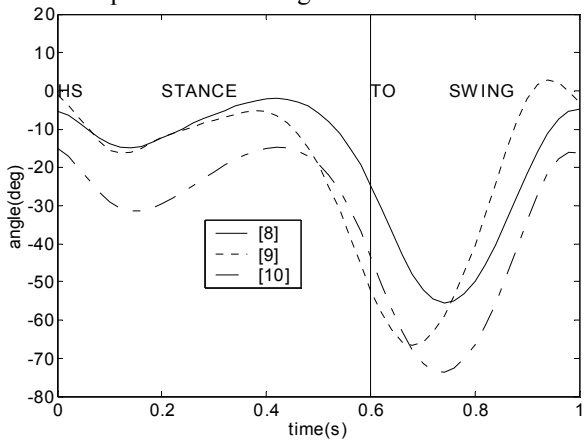

Fig. 7. Adjusted CGA data of the knee flexion/extension angle. The maximum knee angle is ~0˚ (any more would correspond to hyperextension of the knee) whereas the minimum angle is ~-60˚ flexion, occurring in early-mid swing phase enabling the foot to clear the ground.

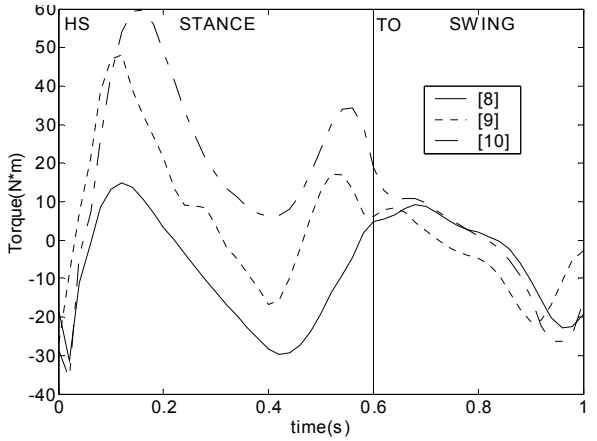

Fig. 8. Adjusted CGA data of the knee flexion/extension torque. An initial ~-35 N·m flexion torque is required at heel strike, followed by large extension torques (~60 N·m) to keep knee from buckling in stance phase.

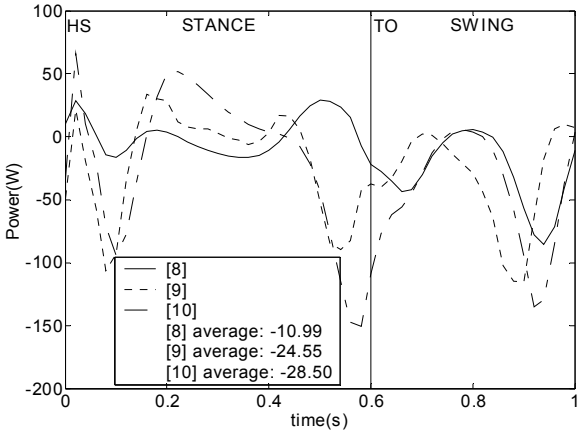

Fig. 9. Adjusted CGA data of the knee flexion/extension instantaneous mechanical power. The negative average indicates power dissipation.

The required knee torque has both positive and negative components, indicating the need for a bi-directional actuator. The highest peak torque is extension in early stance (~60 N·m); hence asymmetric actuators should be biased to provide greater extension torque. Fig. 9 shows the instantaneous mechanical power at the knee, which has both positive and negative components corresponding to power creation and absorption. The average power is negative and therefore the knee (on average) absorbs energy.

D. The Hip

Fig. 10 details the hip angle while walking. The thigh moves in a sinusoidal pattern with the thigh flexed upward at heel-strike to allow foot-ground contact in front of the person. This is followed by an extension of the hip through most of stance phase and a flexion through swing. The BLEEX hip angle is designed to have 10° extension and 115° flexion. The hip torque in Fig. 11 is relatively symmetric (-80 to +60 N·m); hence a bi-directional hip actuator is required. Negative extension torque is required in early stance as the hip supports the load on the stance leg. Hip torque is positive in late stance and early swing as the hip propels the leg forward during swing. In late swing, the torque goes negative as the hip decelerates the leg prior to heel-strike. Fig. 12 shows the instantaneous hip mechanical power. The hip absorbs energy during stance phase and injects it during toe-off to propel the torso forward.

E. Total CGA Power

The total CGA power shown in Fig. 13 was found by summing the absolute values of the instantaneous CGA powers for each joint (Fig. 6, Fig. 9 and Fig. 12) over both legs. The data in Fig. 13 shows that an average of 127W to 210W of mechanical power (i.e. torque x speed) is required to move a 75-kg exoskeleton. This is independent of the type of power source. The absolute value of the joint powers in Fig. 6, Fig. 9 and Fig. 12 was used as a conservative measure (we assumed negative mechanical power in the exoskeleton does not indicate power regeneration). Since the opposite leg is phase shifted by half a cycle, the total CGA power in Fig. 13 has two peaks.

F. BLEEX range of motion

Several mock-ups (one is shown in Fig. 14) were designed and constructed not only for ergonomic evaluation but also for measurement of required range of motion. In particular these mockups were effective in determining the minimum required range of motion of each joint to allow sufficient maneuverability for common tasks such as walking, stair-climbing [7] and squatting. An average person can flex their ankles anywhere from -38° to +35°, their knees to 159° (while kneeling), and their hips to 113° (while prone) [6]. BLEEX's required ranges of motion were set at ±45° ankle flexion/extension, 5° to 126° knee flexion, and 10° hip extension to 115° hip flexion. Extensive experiments showed that increased ankle flexion/extension were needed in the exoskeleton to compensate for the lack of several smaller degrees of freedom in the BLEEX foot. Both the knee and hip ranges of motion were selected to allow

squatting.

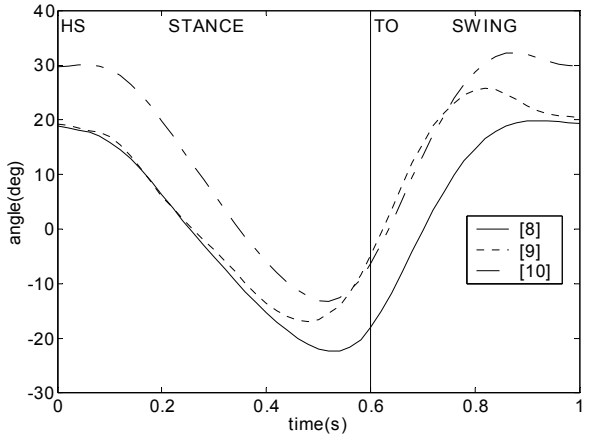

Fig. 10. Adjusted CGA data of the hip flexion/extension angle. The hip has an approximately sinusoidal behavior with the thigh oscillating between being flexed upward ~+30˚ to being extended back ~-20˚.

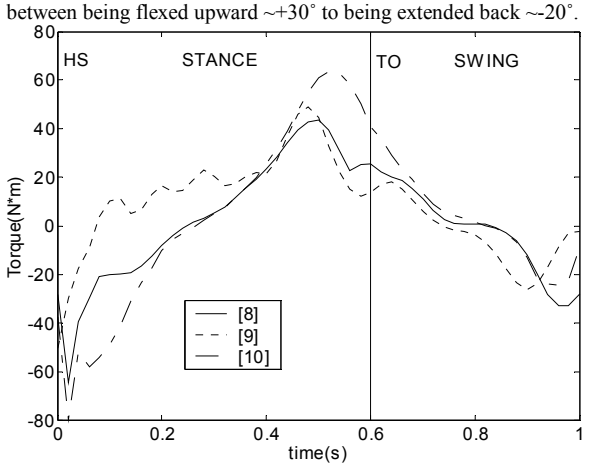

Fig. 11. Adjusted CGA data of the hip flexion/extension torque. The hip torque is bi-directional (~-80 N·m extension to ~+ 60N·m flexion).

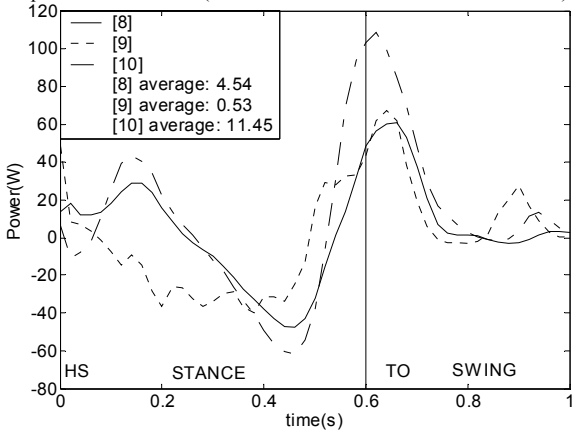

Fig. 12. Adjusted CGA data of the hip flexion/extension instantaneous mechanical power.

G. *Actuation Selection & Modeling*

Electric actuators were ruled out by weight and size restrictions, and pneumatic actuators eliminated by their poor efficiency and controllability [11]. Bi-directional linear hydraulic actuators were chosen as lightweight yet controllable alternatives. Fig. 15 depicts schematic of such an actuator. The magnitudes of the maximum static pushing and pulling forces ($F_{maxpush}$ & $F_{maxpull}$) that can be applied by a bi-directional actuator are given by (1) and (2) as a function of supply pressure (P_{supply}), actuator bore diameter (actD), and rod diameter (rodD).

$$F_{\max\ push} = \mathrm{P}_{\mathrm{supply}} \cdot \frac{\pi(actD)^2}{4} \quad (1)$$

$$F_{\max\ pull} = \mathrm{P}_{\mathrm{supply}} \cdot \frac{\pi\left(actD^2 - rodD^2\right)}{4} \quad (2)$$

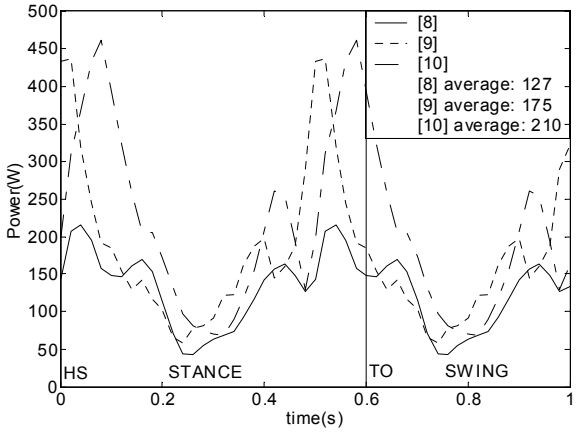

Fig. 13. Total required mechanical power of a 75 kg human walking over flat ground at approximately 1.3 m/s. This was calculated by summing the absolute values of the mechanical powers for the ankles, knees and hips.

Fig. 14. One of the functional mock-ups of the exoskeleton architecture created at UC Berkeley to determine necessary degrees of freedom, ranges of motion, and ergonomic attachments. These prototypes were made by a Fused Deposition Modeling (FDM) machine.

Fig. 15. Bi-directional linear hydraulic actuator schematic. Note that the area on which the internal pressure can act is different on the piston and rod sides of the actuator. This means that the actuator can push with more force than it can pull given the same supply pressure.

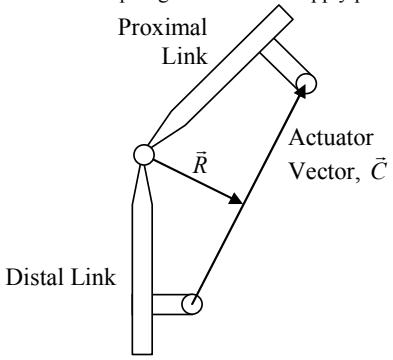

Fig. 16. Triangular configuration of a linear hydraulic actuator.

Fig. 16 shows a linear hydraulic actuator arranged to produce a joint torque. Vector expressions for the

maximum possible torque from an extending and a contracting actuator (T_{push} & T_{pull}) are given by (3) and (4):

$$\vec{T}_{push} = F_{\max\ push}\,\vec{R} \times \frac{\vec{C}}{|C|} \quad (3)$$

$$\vec{T}_{pull} = F_{\max\ pul}\,\vec{R} \times \frac{\vec{C}}{|C|} \quad (4)$$

$\vec{C}$ is a vector whose magnitude is the length of the actuator.

H. Actuation Design Synthesis and Iteration

Fig. 16, (3), and (4) show that the placements of the actuator end points have a direct effect on the magnitude of the joint actuator torque. The farther the actuator is from the joint, the larger the actuator torque and volumetric displacements for a given angular joint motion. Similarly, actuators with larger cross-sections may produce more force and torque, but will require larger volumetric displacements for a given angular motion. Larger volumetric displacements correspond to higher hydraulic flows and increased power consumption for a given angular motion. The problem of actuation design is to find an actuator (i.e., cross-section area, minimum length, and stroke), location of the actuator end-points on two neighboring links, and a constant supply pressure such that the generated torque for each joint is slightly larger than what is shown by Fig. 5, Fig. 8, and Fig. 11 over the entire range of motion (Fig. 4, Fig. 7, and Fig. 10), and subject to several constraints. These constraints include: 1) The actuators are available in discrete sizes (cross-section, minimum length, and stroke); 2) The minimum angular range of motion for each joint described in Section F needs to be guaranteed; 3) The actuator line of action must not pass through the joint; and 4) No interference between the actuators and the links should take place. In general, there is no unique solution, and there are a large number of feasible possibilities. An initial actuator size (cross-section, minimum length, and stroke), and one of the end-point positions were chosen for each joint. Combined with the required minimum angular range of motion (given in Section F), this determined the second actuator mount point (see graphical synthesis for the ankle in Fig. 17). The available actuator torque from (3) and (4) was then compared with the required torques in Fig. 5, Fig. 8, and Fig. 11. This process was iterated with different actuator sizes and mount points until a solution was found.

Fig. 18, Fig. 19 and Fig. 20 show the torque vs. angle plots of the resulting BLEEX joints compared to human CGA data for the ankle, knee and hip. The actuator limit lines show both the available actuator torque and the range of motion of the joint. Fig. 21 shows the physical manifestation of the linear actuator designs evaluated in Fig. 18 through Fig. 20. The ankle requires predominately negative torque (Fig. 5); hence the ankle actuator is positioned anterior to the joint whereby its greater extension force capacity can be exploited. Similarly, the knee actuator is placed behind the knee, where it can apply greater required extension torques (Fig. 8).

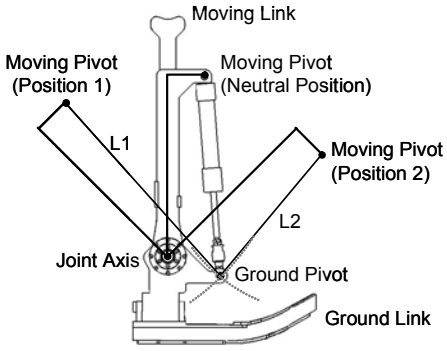

Fig. 17. 2-Position kinematical synthesis of ankle actuator placement. A linear actuator of contracted length L2 and extended length L1 was chosen. The position of the moving pivot in the neutral position was chosen. This defined the moving pivot location at the limits of motion (positions 1 & 2). The position of the ground pivot was found by intersecting arcs of radii L1 and L2 centered at the moving pivot positions 1 & 2.

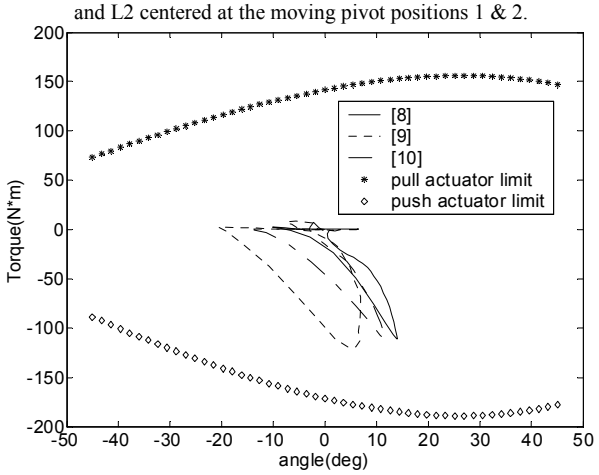

Fig. 18. Ankle torque vs. angle. The actuator torque limits at 1000 psi exceed the adjusted CGA torque of Fig. 5 over the entire range of motion.

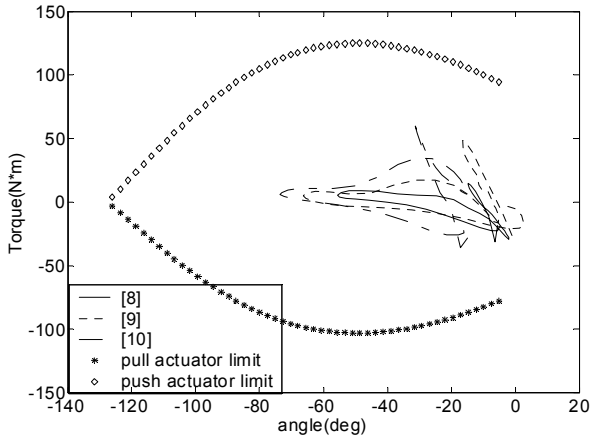

Fig. 19. Knee torque vs. angle. The actuator torque limits at 1000 psi exceed the adjusted CGA torque of Fig. 8 over the entire range of motion.

I. BLEEX Hydraulic Flow and Power Consumption

The total required hydraulic flow shown in Fig. 22 is the sum of the hydraulic flows to each actuator. Individual actuator flows were found by multiplying the magnitude of the actuator linear velocity by the effective area of the actuator over a walking cycle, as shown in (5) and (6). Due to asymmetry, the flow while extending ($Q_{extension}$) differed from that while contracting ($Q_{contraction}$).

$$Q_{extension} \approx ABS\left[\left(\frac{\partial}{\partial t}\left|\vec{C}\right|\right)\cdot\frac{\pi(actD)^2}{4}\right] \quad (5)$$

$$Q_{contraction} \approx ABS\left[\left(\frac{\partial}{\partial t}\left|\vec{C}\right|\right)\cdot\frac{\pi\left((actD)^2-(rodD)^2\right)}{4}\right] \quad (6)$$

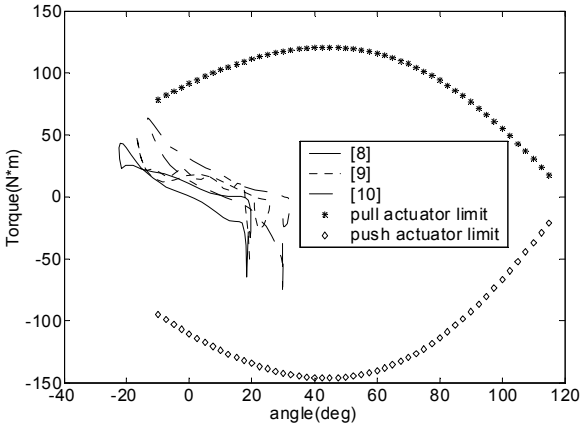

Fig. 20. Hip torque vs. angle. The actuator torque limits at 1000 psi exceed the adjusted CGA torque of Fig. 11 over the entire range of motion.

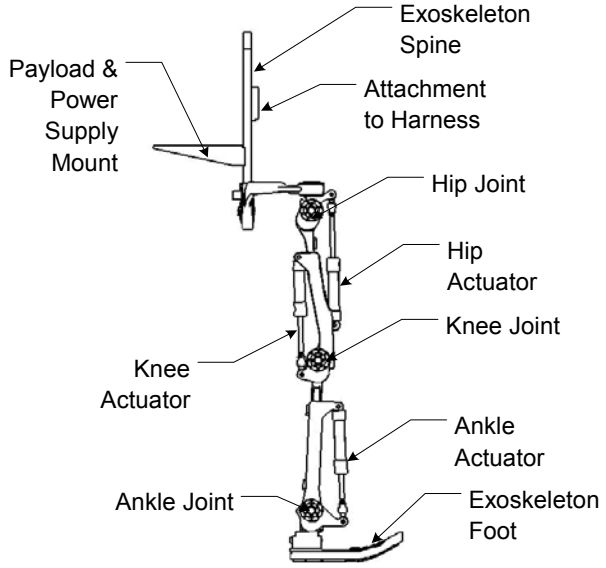

Fig. 21. Model of 1st Generation BLEEX Prototype. This model shows the locations and orientations of the linear hydraulic actuators that support the weight of the exoskeleton and payload.

The total hydraulic power consumption of BLEEX was estimated by multiplying the supply pressure (1000 psi) by the total required hydraulic flow as shown Fig. 23. Fig. 23 predicts a required 1.1-1.3 kW of hydraulic power (pressure·flow) for the BLEEX to walk. This is anywhere from 5 to 7 times the average total mechanical power (torque·speed) shown in Fig. 13. The information shown in Fig. 13 represents the mechanical power needed for a 75-kg person (or 75-kg exoskeleton) to walk according to the CGA data while the data of Fig. 23 represents the hydraulic power for such exoskeleton. The difference between them is the losses due to pressure modulation in the servo-valves. In calculation of the hydraulic power, we considered a constant pressure (1000 psi); however, this constant pressure is reduced in the servo-valve to produce the proper amount of pressure for the actuators. The difference between hydraulic power consumed and mechanical power produced is wasted across the servo-valves. A hydraulic actuator operating at a fraction of its maximum torque capacity consumes the same hydraulic power as if producing its full torque capacity over the same trajectory.

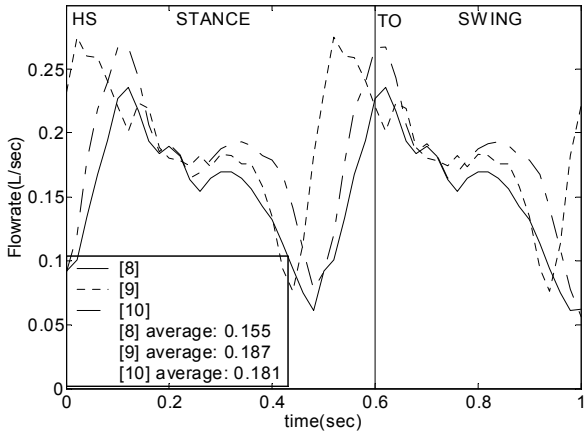

Fig. 22. BLEEX computed instantaneous total required hydraulic flow based on CGA data. Note that this data does not account for leakages.

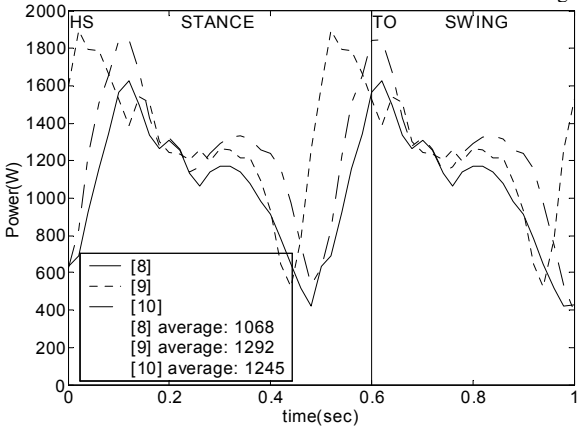

Fig. 23. BLEEX computed total hydraulic power consumption based on human CGA data.

Although Fig. 23 shows that the BLEEX actuators require nominally 1.1-1.3 kW of hydraulic power to walk, more power is required for a successful implementation. The driving 2nd-stage of each of the eight servovalves required an additional approximately 28 W, leading to a total of 240 W of additional hydraulic power consumption. Further analysis also indicated an additional 540W of hydraulic power was required for some activities other than walking (i.e. climbing stairs or ramps) and hip abduction actuators in non-sagittal plane. An estimated 200 W of electrical power was also required by the BLEEX control, sensors, servo-valves, and all electrical subsystems. The net power requirements of the BLEEX after addition of a 10% safety factor were determined to be ~2.27 kW (3 HP) of hydraulic power and 220 W of electrical power. This means 5.2 gpm (20 LPM) of hydraulic flow at 1000 psi (6.9 MPa). A small novel portable power source was designed to produce the required hydraulic and electric power for BLEEX [in print]. Hydraulic actuation and power supply requirements gleaned

from the analysis above were used to design the prototype shown in Fig. 24. The linear hydraulic actuation sizes and placements evaluated in Fig. 18- Fig. 21 were implemented. The estimated hydraulic fluid flow rates estimated by (5) and (6) were used to size both the servo-valves and the hydraulic lines of the system.

Fig. 24: One of the Berkeley Lower Extremity Exoskeleton Prototypes
http://bleex.me.berkeley.edu/bleex.htm

V. Conclusion and Future Work

BLEEX is the first load-bearing and energetically autonomous lower extremity exoskeleton; it has been demonstrated both in the laboratory and outdoor environments. It does not rely on human sensing while still maintaining human operator control (no pre-defined gaits). BLEEX is currently the strongest, successfully walking, untethered lower extremity exoskeleton in existence, and has been worn on a treadmill at speeds up to 1.3 m/s. Development of the exoskeleton is ongoing in Berkeley. Current work includes a more extensive energetic analysis, characterizing dynamical and energetic differences between the actual hardware and CGA data estimates, and design modifications necessary for a 2nd generation prototype. It is hoped that further improvements to both the efficiency and reliability of BLEEX will result in a viable means of material transport over rugged and enclosed terrain.

References

[1] Raibert, M. "Legged Robots", in Legged Robots That Balance, Communications of the ACM, Vol. 29, No. 6, June 1986

[2] Vukobratovic, M., Ciric, V., Hristic, D., "Controbution to the Study of Active Exosksltons", Proc. Of th e5th IFAC Congress, Paris, 1972.

[3] Hristic, D., Vukobratovic, M., "Develop[ment ofActive Aids for Handicapped", Proc. III International Conference on _bio-Mediacl Engineering, Sorrento, Italy, 1973.

[4] Hirai, K., Hirose, M., Haikawa, Y., Takenaka, T., "The Development of Honda Humanoid Robot", in Proc. of the 1998 IEEE International Conference on Robotics & Automation, Leuven, Belgium, 1998.

[5] Rose, J., Gamble, J. G., 1994, *Human Walking*, Second Edition, Williams & Wilkins, Baltimore, p. 26.

[6] Woodson, W., Tillman, B., Tillman, P., "Human Factors Design Handbook", New York: McGraw-Hill, 1992, pp. 550-552.

[7] Riener, R., Rabuffetti, M., Frigo, C., "Stair Ascent and Descent at Different Inclinations", Gait and Posture, vol. 15, pp. 32-34, 2002.

[8] Kirtley, C., CGA Normative Gait Database, Hong Kong Polytechnic University, 10 Young Adults. Available: http://guardian.curtin.edu.au/cga/data/

[9] Winter, A., International Society of Biomechanics, Biomechanical Data Resources, Gait Data. Available: http://www.isbweb.org/data/

[10] Linskell, J., CGA Normative Gait Database, Limb Fitting Centre, Dundee, Scotland, Young Adult. Available: http://guardian.curtin.edu.au/cga/data/

[11] Granosik, G., and Borenstein, J., "Minimizing Air Consumption of Pneumatic Actuators in Mobile Robots," in Proc. IEEE Int. Conf. on Robotics and Automation, New Orleans, LA., 2004, pp. 3643-3639.

[12] Kazerooni, H., "Human-Robot Interaction via the Transfer of Power and Information Signals," IEEE Trans. on Systems and Cybernetics, V. 20, No. 2, Mar. 1990.

[13] Kazerooni, H., "The Human Power Amplifier Technology at the University of California, Berkeley", Journal of Robotics and Autonomous Systems, Elsevier, Volume 19, 1996, pp. 179-187.

[14] Kazerooni, H., Guo, J., "Human Extenders," ASME J. of Dynamic Systems, Measurements, and Control, V. 115, No. 2(B), June 1993.

[15] Kazerooni, H., Guo, H., "Dynamics and Control of Human-Robot Interaction", American Control Conference, San Francisco, California, June 1993, pp. 2398-2402.

[16] Raade, J., Kazerooni, H., "Analysis and Design of a Novel Power Supply for Mobile Robots", IEEE International Conference on Robotics and Automation, New Orleans, LA, April 2004.

[17] McGee, T., Raade, J., and Kazerooni, H., "Monopropellant-Driven Free Piston Hydraulic Pump for Mobile Robotic Systems", Journal of Dynamic Systems, Measurement and Control, Vol. 126, March 2004, pp. 75-81.

[18] Kazerooni, H., Racine, J.-L., Huang, L., Steger, R., "On the Control of the Berkeley Lower Extremity Exoskeleton (BLEEX)", IEEE Int. Conf. on Robotics and Automation, April 2005, Barcelona.

[19] Kazerooni, H., Snyder, T., "A Case Study on Dynamics of Haptic Devices: Human Induced Instability in Powered Hand Controllers," AIAA Journal of Guidance, Control, and Dynamics, Vol. 18, No. 1, 1995, pp. 108-113.

[20] Kim, S., Anwar, G., Kazerooni, H., "High-speed Communication Network for Controls with Application on the Exoskeleton", American Control Conference, Boston, June 2004.

[21] Kim, S., Kazerooni, H., "High Speed Ring-based distributed Networked control system For Real-Time Multivariable Applications", ASME International Mechanical Engineering Congress, Anaheim, CA, November 2004.

[22] General Electric Co., "Hardiman I Arm Test", General Electric Report S-70-1019, Schenectady, NY, 69.

[23] General Electric Co., "Hardiman I Prototype Project, Special Interim Study", General Electric Report S-68-1060, Schenectady, NY, 1968.

[24] Groshaw, P. F., General Electric Co., "Hardiman I Arm Test, Hardiman I Prototype", General Electric Report S-70-1019, Schenectady, NY, 1969.

[25] Makinson, B. J., General Electric Co., "Research and Development Prototype for Machine Augmentation of Human Strength and Endurance, Hardiman I Project", General Electric Report S-71-1056, Schenectady, NY, 1971.

[26] Mizen, N. J., "Preliminary Design for the Shoulders and Arms of a Powered, Exoskeletal Structure", Cornell Aeronautical Laboratory Report VO-1692-V-4, 1965.

[27] Mosher, R. S., "Force-Reflecting Electrohydraulic manipulator", Electro-Technology, Dec. 1960.

[28] Pratt, J., Krupp, B., Morse, C., Collins, S., "The RoboKnee: An Exoskeleton for Enhancing Strength and Endurance During Walking", IEEE Conf. on Robotics and Aut., New Orleans, 2004.

[29] Kawamoto, H., Sankai, Y., "Power Assist System HAL-3 for gait Disorder Person", ICCHP, July 2002, Austria.

[30] Kawamoto, H., Kanbe, S., Sankai, Y., "Power Assist Method for HAL-3 Estimating Operator's Intention Based on Motion Information", in Proc. of 2003 IEEE Workshop on Robot and Human Interactive Communication, Millbrae, CA, 2003 pp. 67-72